2013

Prediction of the Thermomechanical Behavior of Particle-Reinforced Metal Matrix Composites

Yi Hua
University of Nebraska–Lincoln, yhua3@unl.edu

Linxia Gu
University of Nebraska-Lincoln, gul@fit.edu

Prediction of the Thermomechanical Behavior of Particle-Reinforced Metal Matrix Composites

Yi Hua[1] and Linxia Gu[1, 2]

1. Department of Mechanical and Materials Engineering, University of Nebraska–Lincoln, Lincoln, NE 68588-0656, USA

2. Nebraska Center for Materials and Nanoscience, Lincoln, NE 68588-0656, USA

Corresponding author — Linxia Gu, Department of Mechanical and Materials Engineering, University of Nebraska–Lincoln, Lincoln, NE 68588-0656, USA; tel 402 472-7680, fax 402 472-1465, email lgu2@unl.edu

Abstract
The objective of this paper was to predict the thermomechanical behavior of 2080 aluminum alloy reinforced with SiC particles using the Mori–Tanaka theory combined with the finite element method. The influences of particle volume fraction, stiffness, aspect ratio and orientation were examined in terms of effective Young's modulus, Poisson's ratio and coefficient of thermal expansion (CTE) of the composite. The microstructure induced local stress and strain field was obtained through the numerical models of the representative volume element. Results suggested that particle volume fraction had significant impact on the effective Young's modulus, Poisson's ratio and CTE of the composite. Stiffer particles could improve the effective Young's modulus of the composite, while the overall sensitivity of the effective Poisson's ratio and CTE with respect to the particle stiffness was minimal. Particles with larger aspect ratio generally led to a composite with increased effective Young's modulus, as well as reduced Poisson's ratio and CTE. The overall material properties of the composite were insensitive to the particle aspect ratio beyond 10. The particle orientations significantly impacted the effective material properties of the composite, especially along the longitudinal direction. Random 3D dispersed particles exhibited the effective isotropic behavior, whereas anisotropy has been observed for random 2D and unidirectional aligned particles. Our results could help create tailorable bulk composite.

Keywords: discontinuous reinforcement, microstructures, thermomechanical, finite element analysis, micro-mechanics

1. Introduction

Particle-reinforced metal matrix composites (MMCs) have been used in space, automotive, and aircraft industries due to their lightweight, high-strength and high-temperature capacity [1–5]. The thermomechanical behavior of this two-phase material is regulated by its microstructures such as particle properties, size and distribution. Several models have been developed to predict the effective material properties of particle-reinforced MMCs using the homogenization theories such as Voigt approximation, Reuss approximation, Mori–Tanaka (M–T) method [6], and the interpolative double-inclusion (D-I) method [7]. The M–T theory has been proven to provide reasonable predictions for the effective material properties of two-phase composites. Ziegler et al. [8] used the M–T method to predict the elastic properties of metal/ceramic composites with lamellar microstructures, validated by the experimental data. Doghri and Friebel [9] estimated the effective elasto-plastic properties of SiC whisker-reinforced aluminum matrix composites with various volume fractions, aspect ratios and orientations. The results from the M–T theory were consistent with the experimental data. Duschlbauer et al. [10] presented an extended M–T scheme for modeling the linear thermoelastic and thermophysical behavior of carbon fiber reinforced

copper matrix composites, which in agreement with the finite element simulation results. However, the M–T theory failed to provide good estimates for the localization effect induced by the microstructures.

Finite element method (FEM) is capable of identifying the local response of the material. A common practice to estimate the bulk and local responses of composite material is to use a unit cell reinforced by a single fiber, whisker or particle subjected to periodic and symmetric boundary conditions [11–15]. This FE-based approach demands fine mesh at the reinforcement–matrix interface, which led to the need of high end computer as well as costly computation time. Even so, it failed to capture the effect of complex morphology and spatial distribution of the reinforcement, especially for short fiber or irregular particle reinforced matrix. Segurado et al. [16] developed a unit cell model containing 49 particles to investigate the effect of spatial distribution of particles on the elastic response of MMCs. The particles, modeled as spheres, were incorporated with various level of clustering quantified by a radial distribution function. They observed the significant local stress concentrations depending on the level of clustering. Llorca and Segurado [17] used a unit cell model containing 30 non-overlapping identical spheres to study the tensile deformation of particle-reinforced MMCs. Results showed that the strain
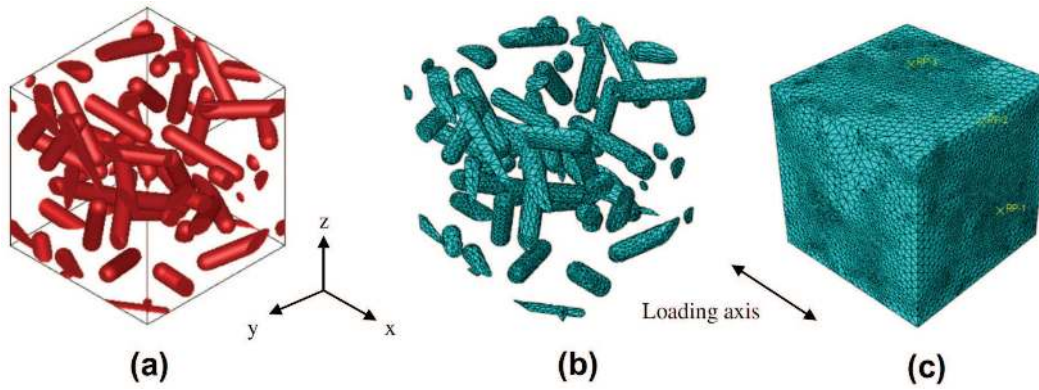
Figure 1. RVE with random distributed sphero-cylinder shaped particles: (a) geometry, (b) meshed particles only, and (c) meshed RVE.
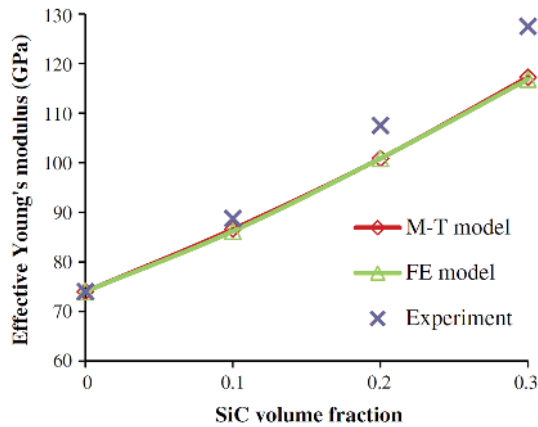

Figure 2. Comparisons among the M–T theory, FE model, and the experimental data [20].

concentration in the matrix was localized in regions between spheres which closely packed along the loading axis. Chawla et al. [18] presented a reconstructed 3D microstructure of SiC particle-reinforced aluminum composites. The localized stress and plasticity was observed due to the sharp and angular nature of irregular particles.

In this work, we combine the computational efficiency of the M–T theory with the local characterization of the FE method to predict the thermomechanical behavior of 2080 aluminum (Al) alloy reinforced with SiC particles. A 3D representative volume element (RVE) containing 30 random distributed particles will be developed to estimate the local and global response of MMCs. The influences of particle volume fraction, stiffness, aspect ratio and orientation will be examined in terms of effective Young's modulus, Poisson's ratio and coefficient of thermal expansion (CTE) of the composite. The stress and strain field around microstructures will be used to enhance the understanding of the global mechanical behavior. This work could help engineer to make design decisions on the composite configuration, and guide to engineering a material's microstructure to obtain desirable characteristics.

2. Finite element modeling

The microstructure of the 2080 aluminum alloy reinforced with SiC particles is represented by a three-dimensional RVE (1 mm each side), as shown in Figure 1a. Thirty identical SiC particles are assumed as sphero-cylinder shape and random dispersed. The particle centers are generated using the random sequential adsorption algorithm [19], with identical probability of orientation. The particle diameter depends on the

particle volume fraction V_p and aspect ratio A_r. In the baseline model, the particle volume fraction is set as 10%, and aspect ratio is chosen as 5. Then the particle diameter is calculated as 0.1 mm. The material properties of SiC particles are adopted with Young's modulus E_p = 410 GPa, Poisson's ratio ν_p = 0.19 and CTE α_p = 4.3e^{-6} K^{-1} [20]. The material properties of Al alloy matrix are taken from published experimental test as E_m = 74 GPa, ν_m = 0.33 and α_m = 2.5e^{-5} K^{-1} [2]. The two phases are meshed with modified 10-node tetrahedral elements with hourglass control (C3D10M), as shown in Figures 1b and 1c. A mesh convergence study is conducted and the minimum mesh size of 0.05 mm is chosen. Periodic boundary conditions are imposed to the RVE faces [21]. A uniform 2% strain is applied to the model along the x-direction. A temperature rise of 100 °C is also applied. The effective material properties of the above described SiC particle-reinforced 2080 aluminum alloy are also predicted using the M–T homogenization theory.

3. Mori–Tanaka theory

The considered RVE (domain ω) contains a matrix phase, denoted by a subscript 0, and an inclusion phase, represented by a subscript 1. The volume fractions (V_i) of these two phases led to $V_0 + V_1 = 1$.

In isothermal linear elasticity, the mean strain over all inclusions is related by [22]

$$\langle \varepsilon \rangle_{\omega_1} = A^\varepsilon : \langle \varepsilon \rangle_\omega = B^\varepsilon : \langle \varepsilon \rangle_{\omega_0} \tag{1}$$

where a colon designates a tensor product contracted over two indices and the brackets $\langle \ \rangle$ represent a volume average. A^ε and B^ε are two strain concentration tensors which have the following relationship:

$$A^\varepsilon = B^\varepsilon : [V_1 B^\varepsilon + (1 - V_1)I]^{-1} \tag{2}$$

where I designates the fourth-order symmetric identity tensor. For M–T model, the strain concentration tensor B^ε is given by

$$B^\varepsilon = H^\varepsilon (I, C_0, C_1) = \left\{ I + \xi_{(I,c_0)} : [(C_0)^{-1} : C_1 - I] \right\}^{-1} \tag{3}$$

where $\xi_{(I,c_0)}$ is Eshelby's tensor and depends on the geometry of inclusion and matrix stiffness. In thermo-elasticity, the mean strain over all inclusions is related to the macroscopic strain E and a uniform change in temperature ΔT as

$$\langle \varepsilon \rangle_{\omega_1} = A^\varepsilon : E + a^\varepsilon \Delta T \tag{4}$$

with A^ε identical to the linear elastic case and

$$a^\varepsilon \equiv (A^\varepsilon - I) : (C_1 - C_0)^{-1} : (\beta_1 - \beta_0) \tag{5}$$
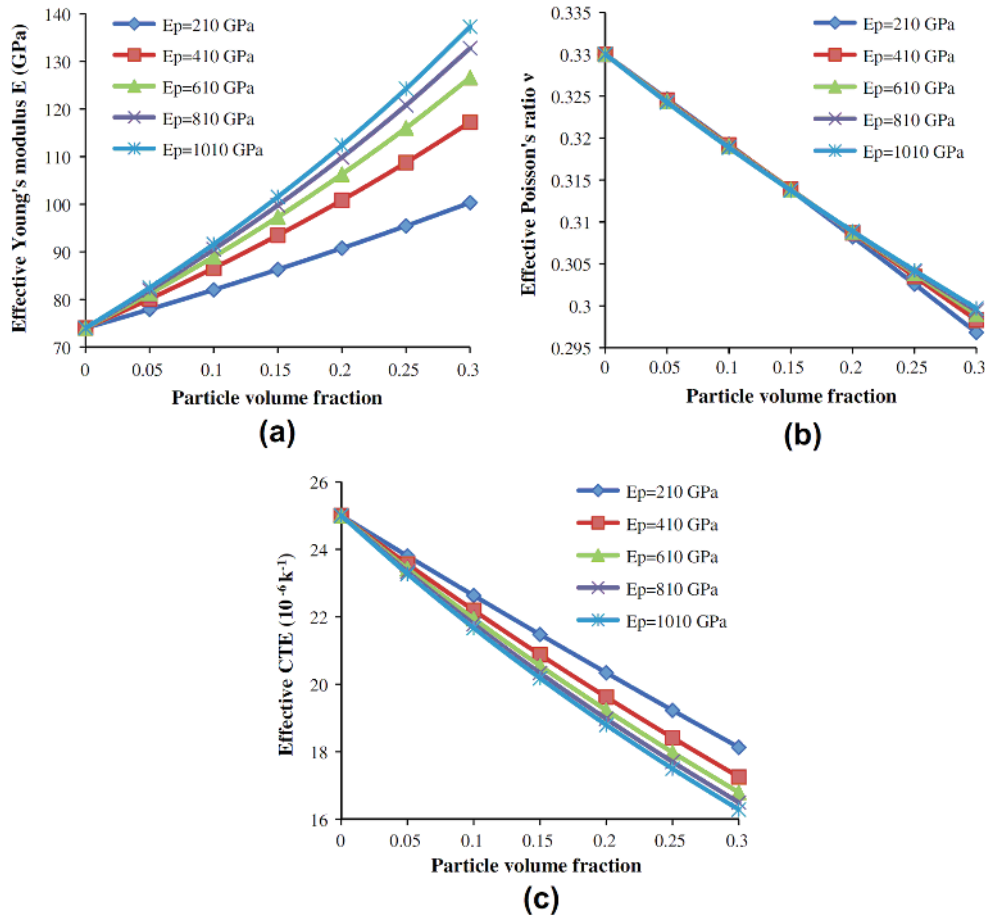
Figure 3. Variation of the effective material properties with change in particle elastic modulus (particle aspect ratio A_r = 5 and orientation of random 3D).
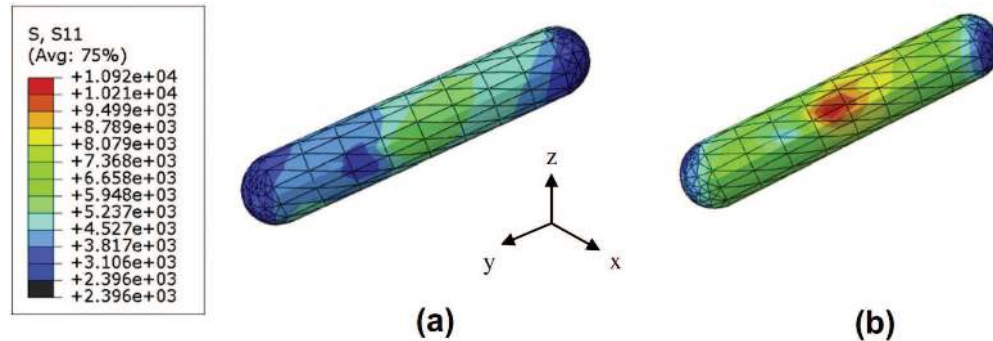

Figure 4. Stress distribution of S_{11} for particles with elastic modulus: (a) E_p = 410 GPa and (b) E_p = 1010 GPa.

$$E = V_0 \langle \varepsilon \rangle_{\omega_0} + V_1 \langle \varepsilon \rangle_{\omega_1} \tag{6}$$

where $\beta = -C{:}\alpha$ and α is the CTE. Per the assumed isotropy, $\alpha_{ij} = \alpha\delta_{ij}$, with δ_{ij} being Kronecker's symbol.

Then the effective bulk response of the composite can be predicted:

$$\langle \sigma \rangle = \bar{C} : E + \bar{\beta}\Delta T \tag{7}$$

where the effective bulk stiffness $\bar{C}$ is obtained as

$$\bar{C} = [V_1 C_1 : B^\varepsilon + (1 - V_1)C_0] : [V_1 B^\varepsilon + (1 - V_1)I]^{-1} \tag{8}$$

and the effective CTE as

$$\bar{\alpha} = -\bar{C}^{-1} : \bar{\beta} \tag{9}$$

where

$$\bar{\beta} = V_0\beta_0 + V_1\beta_1 + V_1(C_1 - C_0) : a^\varepsilon \tag{10}$$

4. Results and discussions

4.1. Validation

The published experimental data on the SiC particle-reinforced 2080 aluminum alloy [20] has been used to validate our M–T and FE models. The comparative results are shown in Figure 2. It is clear that the predictions of the effective Young's modulus of the composite using both M–T and FE models were practically superposed for the particle volume fraction up to 30%. However, the FE analysis was much more time
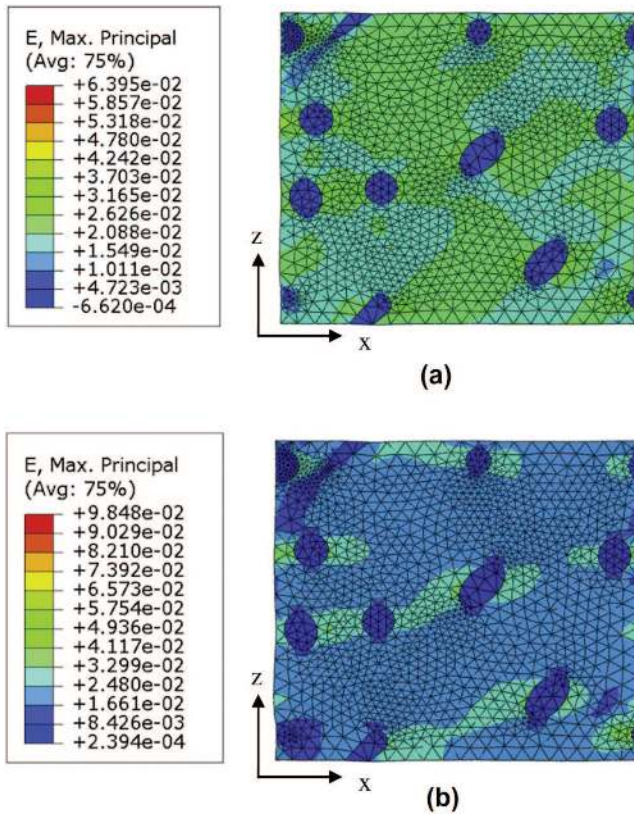
Figure 5. Maximum principal strain distribution in the RVE with particle modulus: (a) E_p = 410 GPa and (b) E_p = 1010 GPa.

consuming, which took over 8750 s for the case of 10% particle volume fraction running on a Dell T3500 double quad-core Xeon W3550 processor, while it only need less than 1 s using M–T method. The results obtained from both M–T and FE models were lower than the documented experimental results. The discrepancies increased with higher particle volume fraction. It was 8.4% with the particle volume fraction of 30%. This could attribute to the numerical simplifications such as constant aspect ratio, idealized 3D random orientation and perfect matrix–particle bonding. A similar underestimate of elastic modulus by simulations has also been observed for the case of unidirectional carbon fiber reinforced silicone matrix subjected to transverse loading [23].

4.2. Influence of particle stiffness

For the random dispersed particles with a fixed aspect ratio of 5, the variation of particle materials (elastic modulus E_p ranging from 210 GPa to 1010 GPa) resulted in the alternations in the effective Young's modulus, Poisson's ratio and CTE of the MMCs (Figure 3). It was observed that the effective Young's modulus of the composite increased with stiffer particle as well as a higher particle volume fraction. The higher sensitivity occurred for particle volume fraction greater than 10%. There was a maximum 36.8% increase in the effective Young's modulus when particle modulus increased from 210 GPa to 1010 GPa at the 30% particle volume fraction. The growth rate in effective Young's modulus decreased with the larger particle modulus. For a particle volume fraction of 10%, the growth rate of effective Young's modulus per every 200 GPa was only 1.2% at the particle modulus of 810 GPa, compared to 5.6% at 210 GPa. Minimal sensitivity of the effective Poisson's ratio with respect to the particle modulus was observed, as shown in Figure 3b. The total increase of the effective Poisson's ratio was only 1.0% at the 30% particle volume fraction when the particle modulus

increased from 210 GPa to 1010 GPa. The decreasing trend in the effective CTE with the higher particle volume fraction was also observed, as plotted in Figure 3c. The CTE decreased approximately 27.5% as the particle volume fraction increased from 0% to 30%. When particle modulus increased from 210 GPa to 1010 GPa, there was a maximum 10.2% reduction in the effective CTE. This could be attributed to the much larger modulus and lower CTE of particles compared to that of metal matrix. The decrease rate of the effective CTE slowed down with the stiffer particle. For the particle volume fraction of 10%, there was only a 0.5% reduction in CTE during the increase of particle modulus from 810 GPa to 1010 GPa, compared to the 1.9% reduction from 210 GPa to 410 GPa.

The influence of particle modulus on the effective Young's modulus, Poisson's ratio, and CTE of the MMCs could be explained by the load sharing capacity of the two-phase material, as presented in Figures 4 and 5, respectively. The microstructures with particle modulus of 410 GPa and 1010 GPa were used to demonstrate the local stress and strain field. The contour plots of the stress component $S11$ along the loading direction (Figure 4) has shown that the stiffer particles shared more loads when the composite subjected to the same external loading, There was a 74.6% increase in the peak stress component S_{11} when particle modulus increased from 410 GPa to 1010 GPa. The maximum stress occurred in the middle portion of the particle, which was consistent with other local stress observations [24]. It was also noted that the maximum principal strain field in the vicinity of particles was up to three times higher than that far away from the particle–matrix interfaces. This highstrain region due to the interface effect enlarged with the increase of particle modulus. This implies a potential early debonding [25].

4.3. Influence of particle aspect ratio

The effective material properties of the composite are also affected by the aspect ratio of the particles A_r, defined by the major diameter vs. minor diameter of the particle. Five composites with various particle aspect ratios (A_r = 1, 5, 10, 15 and 20) were considered here under the condition of having fixed particle modulus E_p = 410 GPa and random 3D distribution of particles. The comparative results of M–T method were shown in Figure 6.

Particles with larger aspect ratio proved to be more efficient in composite stiffness enhancement. As particle aspect ratio increased from 1 to 10 with a particle of volume fraction of 30%, there was a maximum 4.5% increase in the effective Young's modulus, and 1.3% and 3.1% of decreases in the effective Poisson's ratio and CTE, respectively. The material properties of the composite were almost unchanged for particle aspect ratio beyond 10. This saturation of reinforcing effect for large particle aspect ratio was also known as the classic ''shear-lag'' behavior, which described the limiting effect of the small ratio of matrix modulus to particle modulus on the reduction of the load transfer efficiency between phases [26]. In contrast, the effective material properties of MMCs were sensitive to particle volume fraction even with larger aspect ratio. There was a maximum 62.6% increase, 10.5% and 32.1% of decreases in the effective Young's modulus, Poisson's ratio, and CTE, respectively, when particle volume fraction increased from 0% to 30% with the particle aspect ratio of 20.

Probability distributions of stress component S_{11} for particles with aspect ratio A_r = 5 and A_r = 20 was obtained from our FE simulations and shown in Figure 7. It was obvious that the most frequently occurring stress for these two cases appeared within the same range, and this peak probability magnitude increased with a larger particle aspect ratio. The maximum probability of 10.7% occurred at 2125.5 MPa for particles with aspect ratio A_r = 5 and it was 15.7% at 2013.5 MPa for particles with aspect ratio A_r = 20. The tail region of least
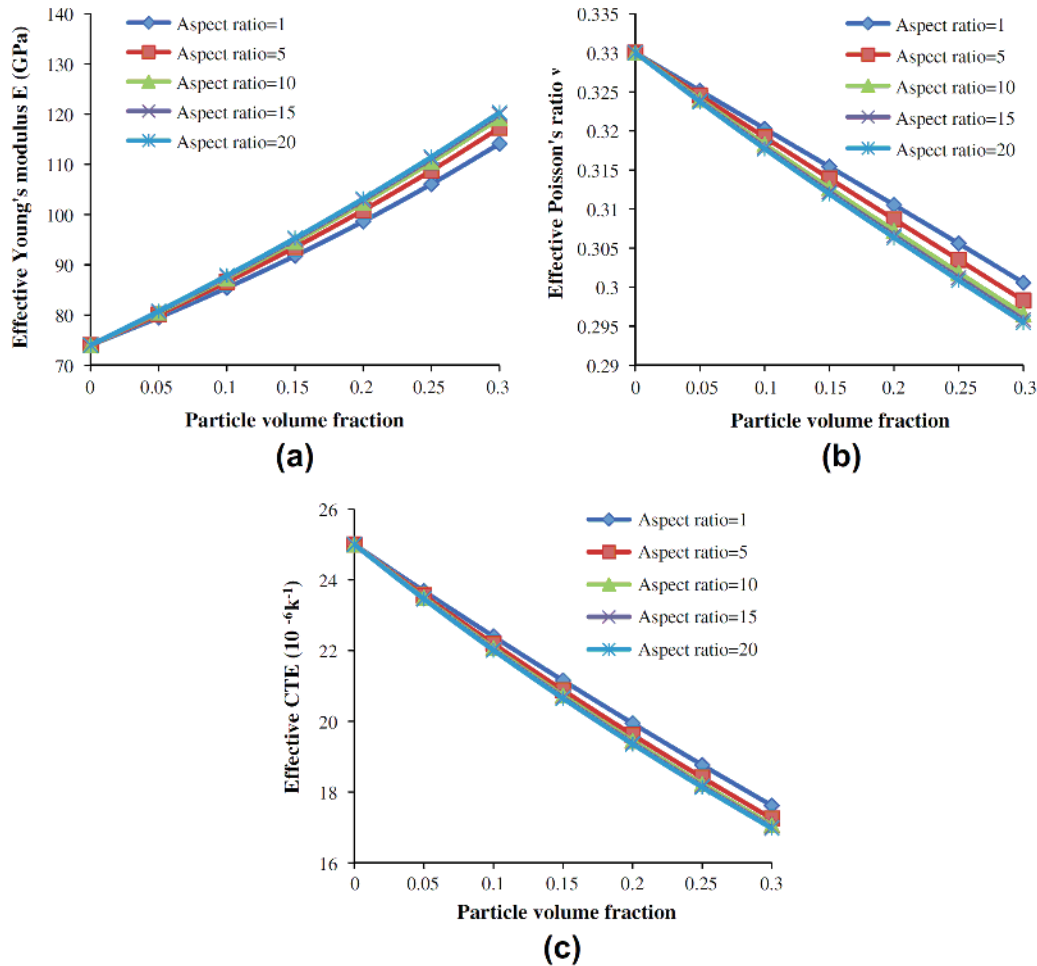
Figure 6. Variation of the effective material properties with change in particle aspect ratio (particle elastic modulus E_p = 410 GPa and orientation of random 3D).
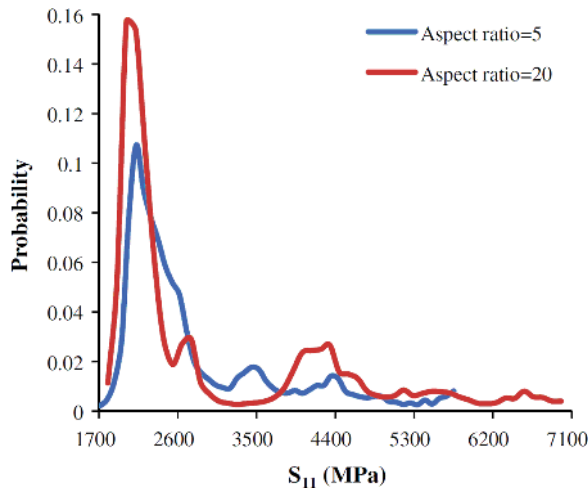

Figure 7. Probability distributions of the stress component S_{11} for particles with aspect ratio A_r = 5 and A_r = 20.

frequently occurring stress values for the composite with particle aspect ratio of 20 extended to 6978.6 MPa, i.e. the peak stress value of the composite, which was 21.3% higher than that with aspect ratio of 5. It demonstrated that the particle aspect ratio significantly altered the peak stress component and the stress distributions.

4.4. Influence of particle orientation

The orientation of the dispersed particles is also an important aspect which could influence the effective material properties of the composite. In this section, we investigated three different particle orientations: perfect alignment, also referred to as unidirection, planar orientation state, also called random 2D, and three-dimensional orientation state, also known as random 3D. The results of M–T method considering constant particle elastic modulus E_p = 410 GPa and aspect ratio A_r = 5 were depicted in Figure 8.

Figures 8a and 8b show the influence of particle orientation on the effective Young's modulus of the composites in the longitudinal and transverse directions, respectively. It was noted that the effective modulus in the longitudinal direction (E_{11}) was strongly dependent on the particle orientation. For the unidirection case, the effective modulus in the longitudinal direction was 19.9% and 26.4% higher than the random 2D and random 3D cases. However the reinforcement of the longitudinal modulus was at the expense of the transverse modulus. The effective transverse modulus for the unidirection case was reduced by 0.8% and 4.7% compared with the random 2D and random 3D cases. The dependence of effective modulus on the particle orientation was much weaker in the transverse direction.

The variation of the effective Poisson's ratio of the composite in both the longitudinal and transverse directions with respect to particle orientations was plotted in Figures 8c and 8d, respectively. It was interesting to note that, in the case of unidirection case, the effective Poisson's ratio ν_{12} increased non-
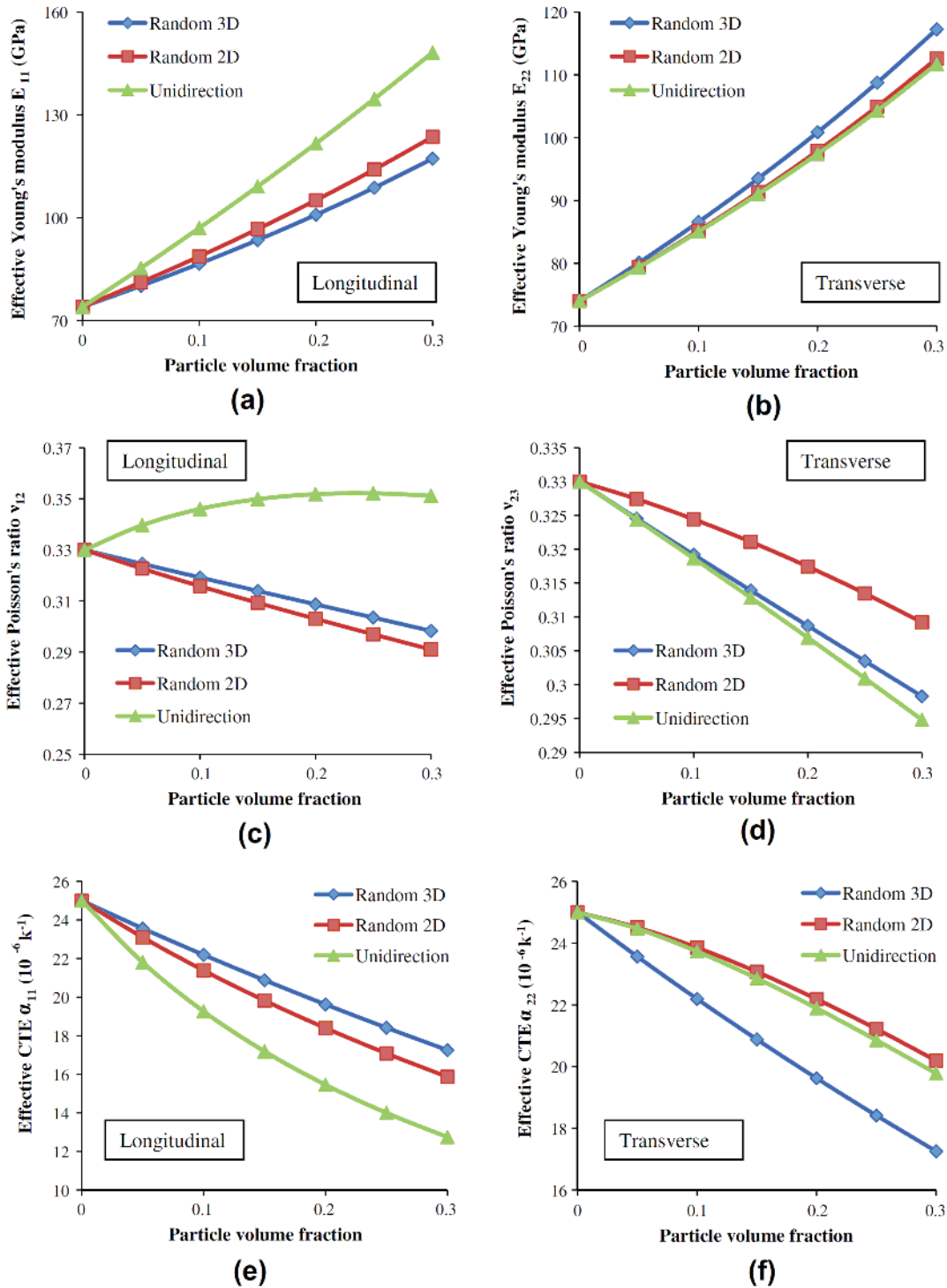
Figure 8. Variation of the effective material properties with change in particle orientation (particle elastic modulus E_p = 410 GPa and aspect ratio A_r = 5).

linearly with the increase of particle volume fraction from 0% to 30%. This nonlinearity was mainly due that the increase in lateral strain was slower than the increase in longitudinal strain. In contrast, this phenomenon did not exist for the 2D or 3D random orientation cases. There was a maximum 11.8% and 9.6% decrease of the effective Poisson's ratio ν_{12} for 2D and 3D random orientation cases, respectively. The effective Poisson's ratio ν_{23} was less sensitive to particle orientations. Compared to particle orientation with random 2D, there was

only a 3.5% and 4.7% decrease in ν_{23} for random 3D and unidirectional states.

Figures 8e and 8f show the predictions of the effective CTE in the longitudinal and transverse directions, respectively. A significant decrease was observed for both α_{11} and α_{22} with the increase of particle volume fraction from 0% to 30%. The longitudinal CTE a11 was more sensitive to particle orientation than the transverse CTE α_{22}. There was a maximum 49.0% decrease of α_{11} for unidirectional state while the maximum

decrease of α_{22} was 31.0% for random 3D state. A definite anisotropy in CTE has been observed for random 2D and unidirectional orientation states. The difference between the longitudinal CTE a11 and transverse CTE α_{22} in these two cases was 35.6% and 21.4%, respectively.

5. Conclusion

The thermomechanical behavior of 2080 aluminum alloy reinforced with SiC particles was investigated through the M–T method. The RVE models were developed to reveal microstructure induced local stress and strain responses for better interpretation of the behavior of MMCs. The modeling framework was verified by the published experiment [20]. The validated model was then used to further characterize the impact of the particle volume fraction, stiffness, aspect ratio and orientation on the macroscopic properties of MMCs.

It was found that particle volume fraction had significant impact on the thermomechanical behavior of the composite. Stiffer particles could improve the effective Young's modulus, while the overall sensitivity of the effective Poisson's ratio and CTE with respect to the particle stiffness was minimal. Particles with larger aspect ratio generally led to a composite with increased effective Young's modulus, as well as reduced Poisson's ratio and CTE. For particle aspect ratio larger than 10, the overall material properties were almost unchanged. The particle orientations strongly impacted the effective material properties of MMCs, especially along the longitudinal direction. Random 3D dispersed particles exhibited the effective isotropic behavior, whereas anisotropy has been observed for random 2D and unidirection orientation cases. It should be noted that the enhancement of MMC behaviors due to the particles with increased stiffness or aspect ratio were at the expense of local stress concentrations, which might initiate the failure of materials.

This work provided a fundamental understanding of the impact of microstructure on the bulk behavior of MMCs, which could be used to guide the optimization of the composite configuration to achieve desirable thermomechanical properties.

References

[1] Chen CH, Cheng CH. Effective elastic moduli of misoriented short-fiber composites. *Int J Solids Struct* 1996;33:2519–39.

[2] Chawla N, Andres C, Jones JW, Allison JE. Effect of SiC volume fraction and particle size on the fatigue resistance of a 2080 Al/SiCp composite. *Metall Mater Trans A* 1998;29:2843–54.

[3] BanksSills L, Leiderman V, Fang DN. On the effect of particle shape and orientation on elastic properties of metal matrix composites. *Compos Part B: Eng* 1997;28:465–81.

[4] Liu FR, Chan KC, Tang CY. Numerical modeling of the thermo-mechanical behavior of particle reinforced metal matrix composites in laser forming by using a multi-particle cell model. *Compos Sci Technol* 2008;68:1943–53.

[5] Chawla N, Shen YL. Mechanical behavior of particle reinforced metal matrix composites. *Adv Eng Mater* 2001;3:357–70.

[6] Mori T, Tanaka K. Average stress in matrix and average elastic energy of materials with misfitting inclusions. *Acta Metall Mater* 1973;21:571–4.

[7] Nemat-Nasse S, Hori M. *Micromechanics: Overall properties of heterogeneous materials.* 2nd ed. Amsterdam: Elsevier Science; 1999.

[8] Ziegler T, Neubrand A, Roy S, Wanner A, Piat R. Elastic constants of metal/ ceramic composites with lamellar microstructures: finite element modelling and ultrasonic experiments. *Compos Sci Technol* 2009;69:620–6.

[9] Doghri I, Friebel C. Effective elasto-plastic properties of inclusion-reinforced composites. Study of shape, orientation and cyclic response. *Mech Mater* 2005;37:45–68.

[10] Duschlbauer D, Bohm HJ, Pettermann HE. Computational simulation of composites reinforced by planar random fibers: Homogenization and localization by unit cell and mean field approaches. *J Compos Mater* 2006;40:2217–34.

[11] Llorca J, Needleman A, Suresh S. An analysis of the effects of matrix void growth on deformation and ductility in metal ceramic composites. *Acta Metall Mater* 1991;39:2317–35.

[12] Brockenbrough JR, Suresh S, Wienecke HA. Deformation of metal–matrix composites with continuous fibers – Geometrical effects of fiber distribution and shape. *Acta Metall Mater* 1991;39:735–52.

[13] Shen YL, Finot M, Needleman A, Suresh S. Effective elastic response of 2-phase composites. *Acta Metall Mater* 1994;42:77–97.

[14] Yuan MN, Yang YQ, Li C, Heng PY, Li LZ. Numerical analysis of the stress–strain distributions in the particle reinforced metal matrix composite SiC/6064Al. *Mater Des* 2012;38:1–6.

[15] Sun CT, Vaidya RS. Prediction of composite properties, from a representative volume element. *Compos Sci Technol* 1996;56:171–9.

[16] Segurado J, Gonzalez C, Llorca J. A numerical investigation of the effect of particle clustering on the mechanical properties of composites. *Acta Mater* 2003;51:2355–69.

[17] LLorca J, Segurado J. Three-dimensional multiparticle cell simulations of deformation and damage in sphere-reinforced composites. *Mat Sci Eng A – Struct* 2004;365:267–74.

[18] Chawla N, Ganesh VV, Wunsch B. Three-dimensional (3D) microstructure visualization and finite element modeling of the mechanical behavior of SiC particle reinforced aluminum composites. *Scripta Mater* 2004;51:161–5.

[19] Widom B. Random sequential addition of hard spheres to a volume. *J Chem Phys* 1966;44:3888–94.

[20] Chawla N, Sidhu RS, Ganesh VV. Three-dimensional visualization and micro structure-based modeling of deformation in particle-reinforced composites. *Acta Mater* 2006;54:1541–8.

[21] Reina-Romo E, Sanz-Herrera JA. Multiscale simulation of particle-reinforced elastic plastic adhesives at small strains. *Comput Methods Appl Mech* 2011;200:2211–22.

[22] Pierard O, Friebel C, Doghri I. Mean-field homogenization of multi-phase thermo-elastic composites: a general framework and its validation. *Compos Sci Technol* 2004;64:1587–603.

[23] Jimenez FL, Pellegrino S. Constitutive modeling of fiber composites with a soft hyperelastic matrix. *Int J Solids Struct* 2012;49:635–47.

[24] Sheng N, Boyce MC, Parks DM, Rutledge GC, Abes JI, Cohen RE. Multiscale micromechanical modeling of polymer/ clay nanocomposites and the effective clay particle. *Polymer* 2004;45:487–506.

[25] Mahmoodi MJ, Aghdam MM, Shakeri M. Micromechanical modeling of interface damage of metal matrix composites subjected to off-axis loading. *Mater Des* 2010;31:829–36.

[26] Cox HL. The elasticity and strength of paper and other fibrous materials. *Brit J Appl Phys* 1952;3:72–9.